Journal of Civil Engineering
The Institution of Engineers, Bangladesh
Vol. CE 24, No. 1, 1996

FORMATION OF SHEAR BAND IN PLANE STRAIN COMPRESSION TEST

Siddiquee, M. S. A[1]., Tanaka, T[2]. and Tatsuoka, F[3]

ABSTRACT : The solutions of boundary value problems involving strain softening material property are full of serious difficulties from both modeling of strain-localization and numerical and mathematical points of view. In this paper, a realistic soil model is applied to capture the formation of shear band in a Plane Strain Compression (PSC) test on dense sand with a very high angle of internal friction. The model (Tatsuoka et al., 1993) is based on experimental findings about inherent and induced anisotropies involved in sand. Stress-dilatancy relation is considered through non-associated plastic flow. Mesh size dependent hardening modulus is considered to alleviate the mesh size dependency of the solution. In the simulations shear band formed without the introduction of any physical defects. It is found that numerical precision error is sufficient to trigger the formation of shear band. Different mesh sizes, advantage of symmetry and boundary conditions are tested numerically to check the formation of shear band. It is found that mesh size, domains taken for the analysis and boundary condition has profound effect on the formation of shear band in PSC test. The result of simulation are compared with that of the experiments.

KEY WORDS : Shear band, PSC test, FEM Simulation

INTRODUCTION

The straightforward use of the strain softening model in a classical continuum generally does not result in a well-posed problem. The field equations that describe the motion of the body lose *ellipticity* and become *hyperbolic* as soon as strain softening occurs. In the eliptic zone, the wave speeds become imaginary and the localization zones stay confined to a line with zero thickness (in 2D case) and the energy consumption in this zone remains zero. These results are in contradiction with experimental data, where a shear band (mode-II) localization shows a finite width of localized zone and a finite value for the consumption of energy. The finite element solution tries to capture the localization zone of zero thickness, which results in a *mesh-*

1 Bangladesh University of Engineering and Technology, Bangladesh
2 Meiji University, Japan
3 The University of Tokyo, Japan

sensitivity. There are several techniques (Needleman, 1988), which are discussed in the review section, employed to obtain mesh size independent shear banding. In this paper, the simplest model is adapted with a view that other affecting factors are equally important in triggering and capturing shear band.

A material model for a granular material with a very high angle of internal friction was used with the features of (1) highly non-linear pre-peak stress-strain relation including inherent and induced anisotropies, (2) non-associated flow characteristics, (3) post-peak strain softening, and (4) strain-localization into a shear band with a specific width (Siddiquee, 1991, Tatsuoka et el., 1991). Inherent and induce anisotropies include the strength anisotropy and pressure-sensitivity of the deformation and strength characteristics of sand respectively. The material model will be briefly described in the later section.

The formation of shear band is obtained without any introduction of weak zone or defects in the description of the mesh. It has been observed in the numerical simulation that mesh size, domains taken for the analysis and boundary condition has profound effect on the formation of shear band in PSC test. The result of simulation are compared with that of the experiments.

REVIEW

Review is concentrated on the formation of shear band. It is a well known fact that strain softening material yields mesh sensitive solutions. Several techniques have been proposed to bypass these unacceptable mesh-dependency. The methods are,

Mesh size dependent hardening modulus

This method employs a mesh-size dependent hardening modulus so as to obtain mesh-independent objective solutions. This procedure appears to have been first proposed by Pietruszcak and Mroz (1981), and has been employed by a number of authors, notably Willam et al. (1984, 1985), A simplified version of this method is used in this study after Tanaka et al. (1990). This model is also used in mode-I fracture in the name of *Fracture energy model* in Bazant and Oh (1983). The model is based on the assumption that the area under the softening curve can be regarded as a material parameter. In order to guarantee a mesh-objective consumption of energy, the softening modulus is made a function of the element size. This kind of shear banding model can incorporate a characteristics length of shear band in the material description and this can be based on the important experimental observation of localization that it has a finite size. The width of localization zone W_s is determined

experimentally, for instance for concrete $W_s = 2.7d_a$, in which d_a is the maximum aggregate size (Bazant and Pijaudier-Cabot, 1989) and for sands $w_s = 10d_g$ -20d_g, in which d_g is the mean grain size diameter (Muhlhaus and Vardoulakis, 1987, Tatsuoka et al., 1994).

Nonlocal Hardening model

These models are basically same as the model described above (mesh size dependent hardening modulus). In this model the internal plastic variable is averaged over a representative volume. This methods provide a localization limiter so that the softening band is restricted to a zone of certain minimum size which is a material property. This concept, originally introduced on the basis of statistical analysis of heterogeneous materials, has been widely applied in elasticity (Eringen and Edelen, 1972). Application of the nonlocal concepts to strain-softening was proposed by Bazant, Belytschko and Chang (1984). It was later simplified by the concept of nonlocal damage (Bazant and Lin, 1988). In this approach the main idea is that only those variables which cause strain-softening are subjected to nonlocal formulation.

Gradient plasticity model

In this method, the continuum description (either stress or strain) is enriched by inclusion of higher-order gradient terms. Spatial derivatives of the inelastic state variables enter the constitutive equations. This approach defines a dependence of the yield function on the second-order gradient of the equivalent plastic strain (Muhlhaus and Aifantis 1991).

Rate-dependent model

An entirely different approach is the inclusion of rate-dependence in the constitutive equations (Wu and Freund 1984, Needleman 1988, Loret and Prevost 1990). Extra higher-order time derivative terms prevent the field equations from becoming elliptic and keep the problem well-posed. Dispersive waves and an implicit length scale enables the rate-dependent continuum to capture localization of deformation.

Micro-polar (Cosserat) continuum model

The micro-polar (Cosserat) continuum model is based on the idea of a micro-structure subdivided into micro elements with rotational degrees of freedom (Cosserat and Cosserat 1909, Gunther 1958, Muhlhaus and Vardoulakis 1987). This model closely connects the heterogeneous character of softening materials as sands, rock and concrete. A length scale is introduced by a finite size of the micro-elements. The regularization effect comes from the introduction of couple-stresses and

micro-rotations, so that extra rotational degrees-of-freedoms are defined.

MATERIAL MODEL

The material model used in this paper is a generalized elasto-plastic, isotropic strain hardening-softening one. It takes into account of strain localization associated with shear banding by introducing a characteristic width of shear band in the additive elasto-plastic decomposition of strain. Unlike the method used by Pietruszczak and Mroz, here no direction of shear banding is specified. Rather, it is implicitly assumed that the direction of shear band coincides in a broad sense with the direction of maximum shear strain. A generalized hyperbolic equation (Tatsuoka et al., 1993) has been used as the growth function of the yield surface. The yield surface used is a generalized Mohr-Coulomb one given by;

$$\phi = \eta I_1 + \frac{1}{g(\theta)} \sqrt{J_2} - K \qquad (1)$$

where I_1 is the first invariant of stress (i.e. hydrostatic stress component), J_2 is the second invariant of deviatoric stress and g(θ) is the Lode angle function which is defined as;

$$g(\theta) = \frac{3 - \sin \phi_{mob}}{2\sqrt{3}\cos\theta - 2\sin\phi_{mob}} \qquad (2)$$

η is the deviatoric stress at $\theta = 30°$ (on the π - plane), which is related to the mobilized angle of internal friction ϕ_{mob} as ;

$$\eta = \frac{2\sin\phi_{mob}}{\sqrt{3}(3 - \sin\phi_{mob})} \qquad (3)$$

The plastic potential is defined as ;

$$\psi = \alpha' I_1 + \sqrt{J_2} - K = 0 \qquad (4)$$

This equation of plastic potential is Drucker-Prager type, and similar to that of yield surface except the difference in that $g(\theta) = 1.0$ in Eq. (1) This equation was employed so as to have differentiability at all stress-states.

The factor α' depends on the type of analysis. As all the analysis was done under plane strain conditions in the present study, the factor α' used was;

$$\alpha' = \frac{\tan\psi}{\sqrt{9 + 12\tan^2\psi}} \qquad (5)$$

where ψ is the mobilized angle of dilatancy, which is given by ;

$$\psi = \arcsin\left(- \frac{d\varepsilon^P_1 + d\varepsilon^P_3}{d\varepsilon^P_1 - d\varepsilon^P_3} \right) \quad (6)$$

where $d\varepsilon_1{}^P$ and $d\varepsilon_2{}^P$ are the major and minor principal strain increments (positive in compression). In this study, the value of ψ was determined from Rowe's stress dilatancy relation (Rowe, 1962).

$$\frac{\sigma_1}{\sigma_3} = - K \left(\frac{d\varepsilon^P_1}{d\varepsilon^P_3} \right) \quad (K = \text{a material constant}) \quad (7)$$

As the model has the yield function and plastic potential surface having different forms, it is one of the non-normal plasticity models, or in other words it is a non-associated flow model (Vermeer and de Borst, 1984).

In the present study, a fine quartz-rich sand (Toyoura sand) was selected as the material to be analyzed. This sand was also used in the model bearing capacity test of footing which will be described later in this paper. The pressure-dependency and inherent anisotropy of the deformation and strength characteristics of air-pluviated Toyoura sand measured under plane strain conditions as reported elsewhere (Tatsuoka et al., 1991) have been implemented into the material model by introducing directly the empirical equations for them (Tatsuoka et al., 1993).

SOLUTION STRATEGY

Solution of systems of nonlinear equations involving the governing non-linear equation is ;

$$P - P^{init} = F$$

$$\text{and } P = \sum_{N} \int_{ve} B \sigma \, dv \quad (8)$$

where P is the internal force vector, P^{init} is the nodal forces due to initial stresses, F is the external force vector, B is the strain-displacement transformation matrix, N is the number of elements in FEM discretization, σ is the stresses in each element at Gauss points and Ve is the volume of each element.

The solution to the above governing equation can be obtained by achieving the steady state response of the following dynamic equation of motion (Zienkiewicz, 1984);

$$m\ddot{u} + c\dot{u} + p - P^{init} = F \tag{9}$$

where **m** is the diagonalized mass matrix, c is the damping matrix, which is a vector for critically damped dynamic relaxation, $\dot{u}$ is the velocity vector and $\ddot{u}$ is the acceleration vector.

Then, applying the central difference technique to Eq. (9) and replacing the damping by the following well-known relation;

$$c = \alpha\, m \tag{10}$$

the following relaxation equation can be derived ;

$$u^{t+\Delta t} = \frac{1}{(1 + 0.5\alpha\Delta t)} \left[\frac{\Delta t^2}{m} (F - P + P^{init})^{t} + 2u^{t} - (1 - 0.5\alpha\Delta t)\, u^{t-\Delta t} \right] \tag{11}$$

Here, α is the damping ratio, which is the most critical value to be determined. Using the following substitutions;

$$\xi = 0.5\alpha t,\ \delta_1 = \frac{1}{1+\xi},\ \delta_2 = 1 - \xi \tag{12}$$

$$m' = \frac{\Delta t^2}{m},\ R^t = (F - P + P^{init})^t$$

Eq. (11) can be rewritten in the following concise form;

$$u^{t+\Delta t} = \delta_1 \,(m' R^t + 2u^t - \delta_2 u^{t-\Delta t}) \tag{13}$$

There are a number of methods that can estimate a reasonable value of the critical damping parameter, α. Some of the methods need some extra iteration to determine the first peak in kinetic energy variation of an undamped free vibration (Ramesh and Krishnamoorthy, 1993). Another method (Bunce, 1972) uses the Rayleigh's quotient to determine the approximate damping in an adaptive way using the current solution parameters. Namely, the Rayleigh's quotient is;

$$\alpha = 2\sqrt{\frac{xKx}{xMx}} \tag{14}$$

where x is the eigen vector, which can be approximated by incremental displacement vector (**u**) and **K** is the global stiffness matrix, which can be approximated by a local tangent stiffness ($\mathbf{K}^{lt}$). Mass matrix **M** can be well approximated by a diagonal matrix, **m**. So the damping ratio α is determined by;

$$\alpha = 2\sqrt{\frac{u\, K^{lt} u}{u\, m\, u}} \tag{15}$$

where the local tangential diagonal stiffness matrix is approximated from the following equation (Underwood, 1983);

$$k^{it} = \frac{t_{P\_1} - \Delta t_P}{\Delta t_u} \tag{16}$$

As DR is based on an explicit integration scheme, it suffers from the stability problem. This instability arises mainly from the mismatch of integration speed to deformation wave speed. Mathematically, this condition can be expressed as :

$$\Delta t \leq \beta = \frac{l}{V_c} \tag{17}$$

where β is a stability enforcing factor (β<1.0), and l is the minimum distance between the adjacent nodal points for an element. For constant strain elements, the value of β can be near 1.0, but for higher order elements it reduces very fast. V_c is the constrained compression wave velocity of the medium, since the pseudo-densities are calculated separately in each of the x and y directions.

Using the expression of the constrained elastic compression wave velocity, V_c, Eq. (17) can be re-written in the following form;

$$\Delta t \leq \beta l \sqrt{\frac{\rho(1+\upsilon)(1-2\upsilon)}{E(1-\upsilon)}} \tag{18}$$

where ρ is the density of the medium, υ is the Poisson's ratio and E is the Young's modulus of the medium. Based on Eq. (18), a scaling method can be introduced, which is essentially a mesh homogenization (Underwood, 1983, Key et al., 1982). In all of the numerical tests described in this paper, the only adjustable DR parameter was β, which was set equal to 0.6 to achieve the stability of the explicit DR computation. All the other parameters were adapted and adjusted automatically throughout the equilibrium iterations. In the displacement control solution, some of the displacement components are fixed during one load step while the others are solved. Equations for fixed displacement components are as follows ;

$$u^{t+\Delta t} = \delta_1 \, (m^t R^t + 2u^t - \delta_2 \, u^{t-\Delta t}) \tag{19}$$

$$R^{t-\Delta t} = 0, \; \delta_1 = \delta_2 = 1.0, \; u^t = u^{t-\Delta t}$$

The other degrees of freedom are solved by Eq. (13) as usual.

PROBLEM SETUP AND ANALYSIS

For a comprehensive analysis of the numerical schemes described in the previous section, a relatively simple problem was selected. In the

context of FEM, it is a 2D domain of PSC test discretized by four noded quadrilaterals (Tanaka and Kawamoto, 1988) (Fig. 1) . The confining pressure σ_3 is constant and equal to 0.8 $\times$98 kPa. The cases analyzed are listed in Table 1.

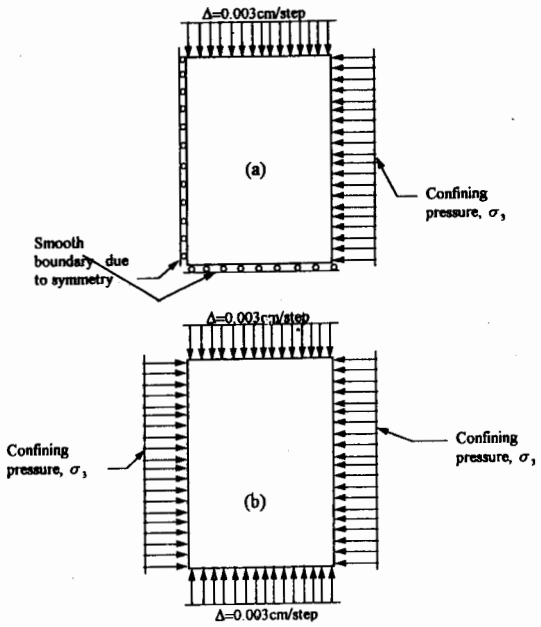

Fig 1. Boundary conditions for (a) symmetrically discretized and (b) full mesh.

Four noded quadrilateral elements in general show a stiff response. In Order to obtain an accurate solution, reduced integration (Zienkiewicz et al., 1971) was used. Reduced integration in a four noded isoparametric element can give rise to a zero-energy mode (hour-glass mode). An anti-hourglass scheme (Flanagan and Belytschko, 1981) was used to prevent any probable hour-glass mode. A careful choice of parameters is required for the hour-glass control in a given materially non-linear analysis. In the present study, an elastic stiffness approach was employed, where a very small elastic stiffness (0.05% of the actual material stiffness) was added to the non-linear system as hour-glass resisting nodal force whenever any element starts to form a hour-glass mode. The approximate parameter was found after some trial runs. Then this procedure prevented effectively a hour-glass mode while it did not increase the stiffness of the solution.

The integration of the elasto-plastic equation was done by the return mapping scheme (Ortiz and Simo, 1986), which is a first-order-approximate Euler backward integration. The stress-strain relation of air-pluviated Toyoura sand to be solved by DR is given in Fig. 2. It was

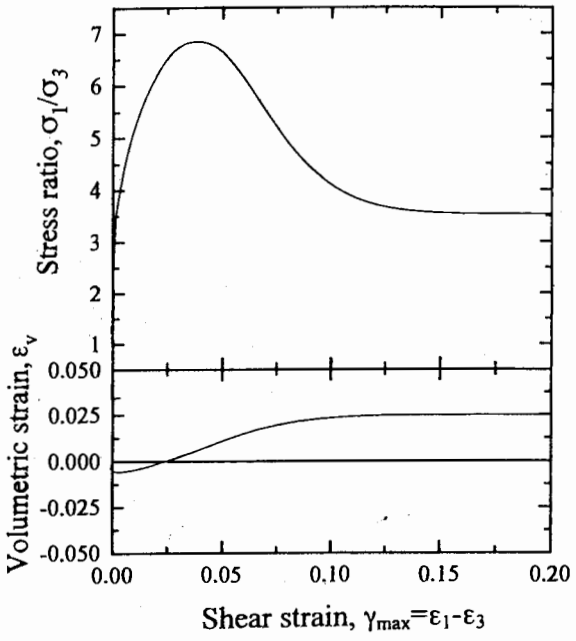

Fig 2. *Stress-strain relationship under plane strain conditions for the model problem.*

assumed that the deformation is homogeneous up to the peak stress state, while strain localization into a shear band starts at the peak stress state. This assumption is based on experimental observations in plane strain compression tests (Tatsuoka et al., 1990). In the post-peak regime, therefore, the deformation of the whole of the element consists of the plastic deformation in the process of loading occurring in the shear band and the elastic rebound of the whole of the element. The post-peak stress strain relations shown in Fig. 2 are those average for the 2.5 cm x 2.5 cm element. As a shear band width of 0.3 cm is assumed in the post-peak regime, the shear strain increment in the shear band is $\sqrt{2}$ (2.5/0.3) times larger than those shown in Fig. 2. The volumetric strain ε_v consists of elastic and plastic parts (i.e. $\varepsilon_v{}^P$), and for a given plastic major principal strain increment $d\varepsilon_1{}^P$, the increment $d\varepsilon_v{}^P$ is obtained by Rowe's stress-dilatancy equation (Eq. 7) with K = 3.5. The peak and

residual angles of friction ϕ_p and ϕ_r were determined based on experimental results (Tatsuoka et al., 1993). The elastic shear modulus, G^e was equal to 7722 kPa, which was obtained by substituting a void ratio e = 0.66 into the empirical relation;

$$G^e = 900. \frac{(2.17 - e)}{(1 + e)^2} \cdot \left(\frac{\sigma_3}{P_a}\right)^{0.4} \cdot P_a \qquad (20)$$

P_a is the atmospheric pressure equal to 98 kPa, The elastic Poisson's ratio equal to 0.3 was used.

The introduction of strain localization is also done by distributing the total width of shear band with one elements' all the gauss points. The following table shows the cases analyzed to assess the properties and suitability of different types of elements. This point was extensibly studied to find the suitable element which can capture the strain localization phenomenon as closely as to the one seen in the PSC experiment.

Table 1 Effect of type of element on PSC solution

Cases	Element Type	Number of nodes	Gauss Points	Stability factor, ρ	Total no. of nodes	Total no. of elements
sqr1	Iso-p element	4	1	0.5	121	100
s400	Iso-p element	4	1	0.5	441	400
sr800	Iso-p element	4	1	0.5	861	800
crstps	Iso-p element	4	1	0.5	221	400
f800	Iso-p element	4	1	0.6	861	800
f800s	Iso-p element	4	1	0.6	861	800

Meshes are shown at the beginning of each figure that will come into discussion subsequently. The boundary conditions are imposed on a quarter of the PSC element test domain (taking advantage of the symmetry) in all cases except case "f800", where a full element is used under a boundary condition (with and without friction) similar to that of the experiment.

RESULTS AND DISCUSSIONS

Fig. 3 shows the result of case "sqr1" with one point reduced integration. In this case due to the coarseness of meshing, a relatively wide shear band is developed. If the mesh is refined further like in Fig. 4 (case "s400"), it shows a completely different picture. Now the boundary

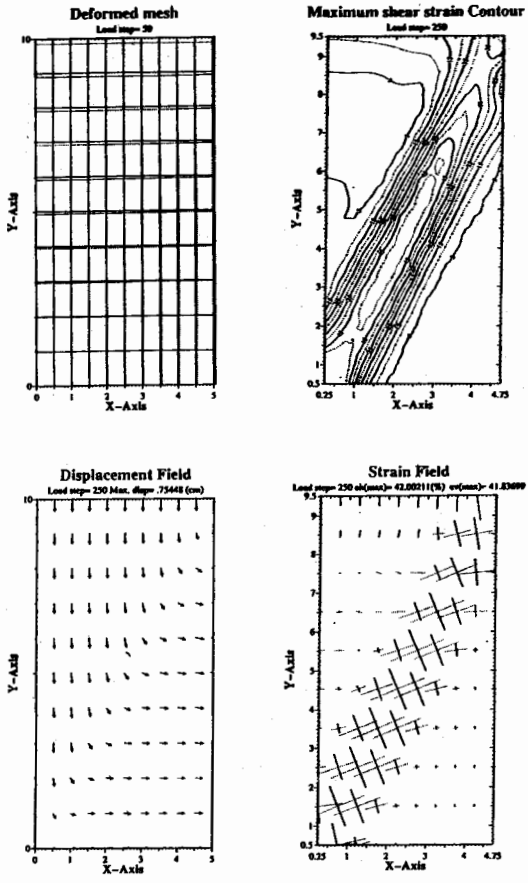

Fig 3. Results of PSC simulation for case "sqr1" consists of four noded elements with one point reduced integration.

condition shows a large effect on the formation of shear band. In fact, a kind of wave reflection is observed at the fictitious boundary, i.e., along the central lines (vertical and horizontal) with the specimen. Fig. 5 shows the sequential development of maximum shear strain, γ for the case "s400". A clear rebound type multiple shear banding is observed mainly due to the boundary effect as shear band tries to form across the whole element. Fig. 6 is the result of case "sr800" which is further refined mesh with the same four-noded element with one- point reduced integration. The shear banding has a similar feature of multiple shear banding probably due to the smooth kinematically constrained boundary condition imposed from symmetry.

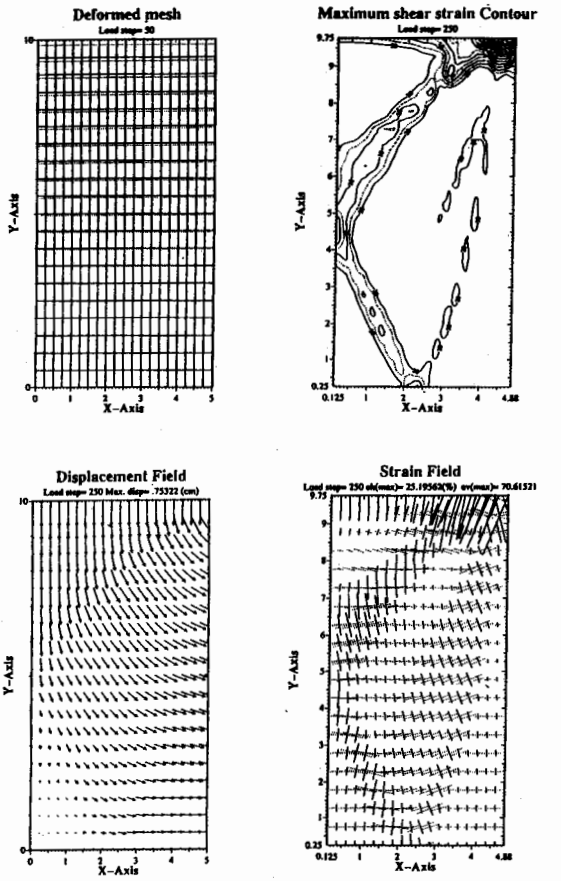

Fig 4. Results of PSC simulation for case "s400" consists of four noded elements with one point reduced integration.

Fig. 7 shows the result of case "crstps", which consisted of crossed triangular elements. This kind of element is considered to be effective for capturing strain localization (Heinstein and Yang, 1992). The result shows a better capturing of shearband but a reflective nature of multiple shear banding is clearly formed. From Fig. 8, the sequential development of maximum shear strain, γ, is noticed to be formed at different rates, confirming its reflective nature.

Fig. 9 shows the result of case "f800" (frictional ends), whichconsisted of four-noded quadrilateral with one-point reduced integration. This mesh is designed to be full (not taking advantage of the symmetry of loading) in order to study into the shear band reflection in the case of quarter-domain analysis. It is very interesting to note that in this case a

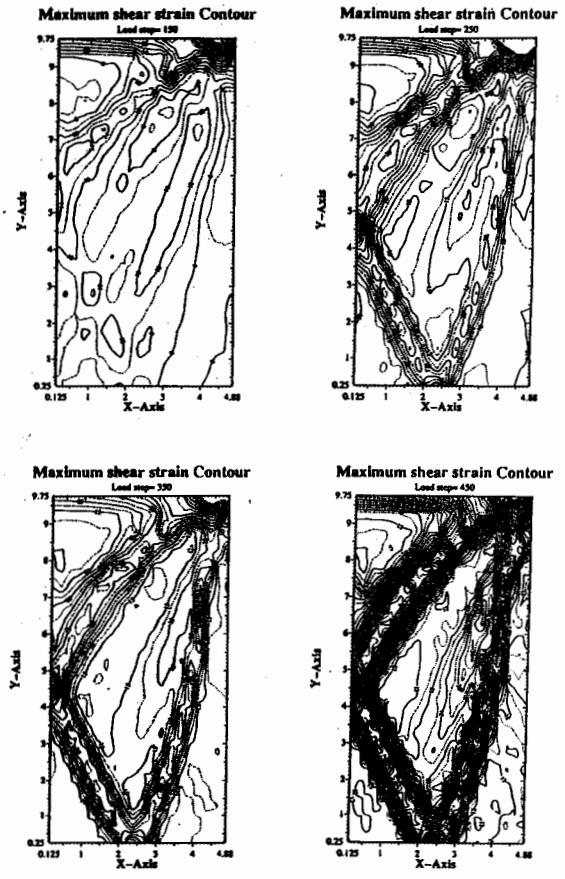

Fig 5. Sequential development of maximum shear strain γ showing the formation of shear band for case "s400".

pair of very clear and relatively sharp (as much as allowed by iso-parametric element) shear bands are formed without any refletion or multiple shear band. All the analysis were performed without applying any kind of imperfection (neither geometric nor material imperfection). The reason of the localization without introducing any imperfection may be attributed to the numerical truncation error, which provides a pseudo-random distribution of stress-state with a very narrow range of variation (of the order of the tolerance of the analysis, 10^{-6}) multiple shear band. All the analysis were performed without applying any kind of imperfection (neither geometric nor material imperfection). The reason of the localization without introducing any imperfection may be attributed to the numerical truncation error, which provides a pseudo-

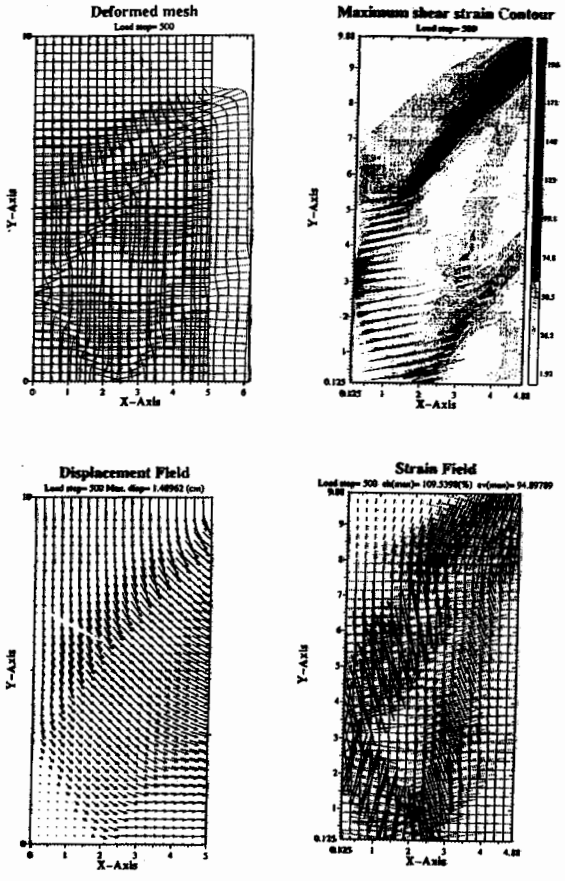

Fig 6. Results of PSC simulation for case "sr800" consists of four noded elements with one point reduced integration.

shows the meshes after sequential development of deformation, which shows a clear shear band formation-direction close to the analytical Roscoe solution (the diretion of zero-extension line at the peak state). Fig. 11 shows the corresponding maximum shear strain contours. It can be seen from the figures that initially localization started from four corners (singular points) but did not have further development. Subsequently the location of strain concentration shifts to the center of the specimen. At a loading step of 250, the average axial strain, ε_a = 7.5% (n.b. the peak axial strain = 2.2%). In this analysis, the peak and residual

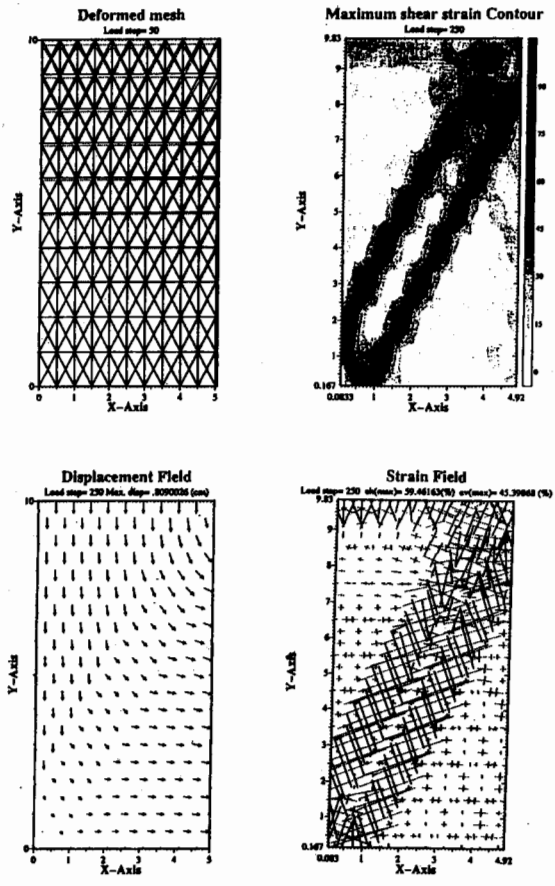

Fig 7. Results of PSC simulation for case "crstps" consists of crossed triangular elements with one point reduced integration.

angles of internal friction, φ_r = 34° and φ_{peak} = 47.17° (for σ_3 = 0.8 kgf/cm^2) are used. It is seen that the theoretical perfect plasticity solution of shear band, i.e., the Roscoe surface at an angle of $(\pi/4 + \psi/2)$ = 45° + 13.17/2 = 51.58° is exactly simulated.

Fig. 11 through 15 show the results of case "f800s", which consisted of four-noded quadrilateral with one-point reduced integration. This mesh is designed to be full (not taking advantage of the symmetry of loading) in order to study the shear band reflection in the case of quarter-domain analysis and top, bottoms are made perfectly smooth. This resulted in a single shear band without introducing any kind of imperfection. Figs. 11

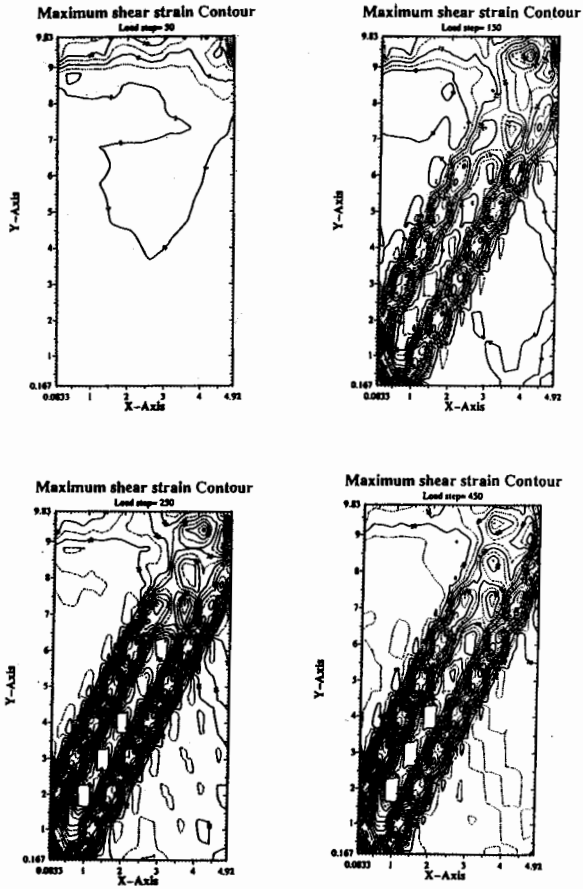

Fig 8. Sequential development of maximum shear strain, γ showing the formation of shear band for case "crstps".

through 15 show the sequential development of deformed mesh, maximum shear strain contours, displacement fields and strain fields respectively. They all focus on showing how a single shear band developed by simulating a plane strain condition without introducing any kind of imperfection other than the material model itself. Fig. 16 compares the FEM simulation with PSC experiments performed with Toyoura sand and glass beads (n.b., the FEM simulation is made for the conditions of PSC test using Toyoura sand). It is interesting to note that glass beads has a larger mean particle diameter compared to Toyoura sand resulting in a larger shear band width and a lesser angle of localization zone. In the FEM simulation, due to the inability of iso-

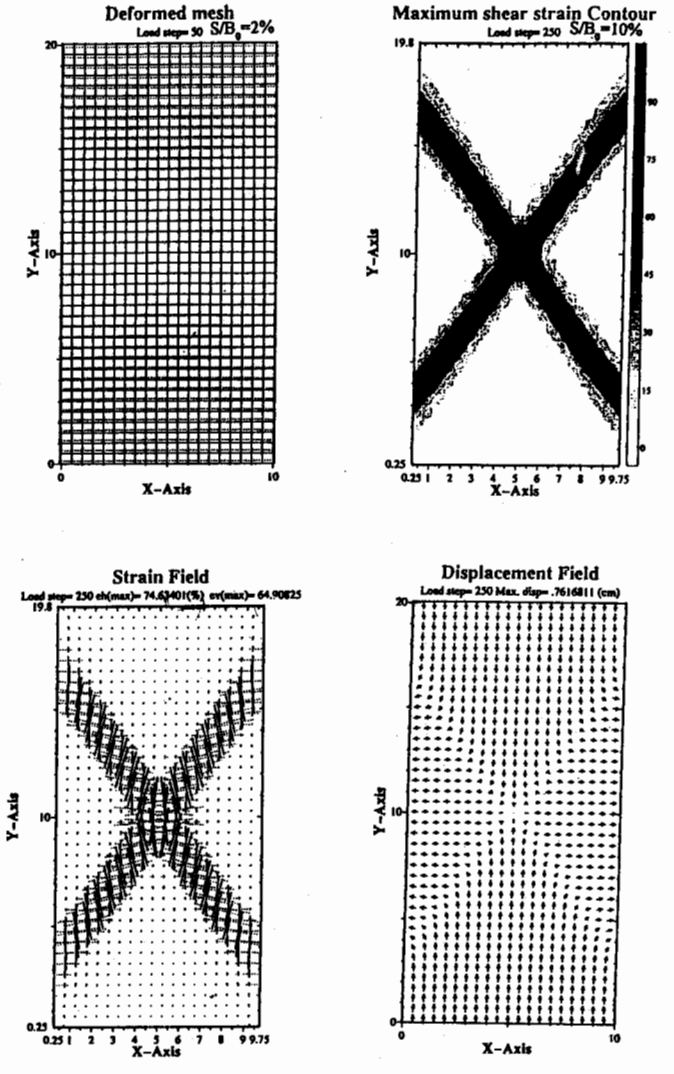

Fig 9. Results of PSC simulation for case "f800" consists of four noded elements with one point reduced integration (full mesh).

parametric 4-noded element to deform with a strain jump inside the element (i.e., strain localization into a narrower shear band), a several element width is needed to form the localization zone. Consequently, a shear band of a larger diameter material (i. e., glass beads) resembled the FEM simulation of PSC test on Toyoura sand.

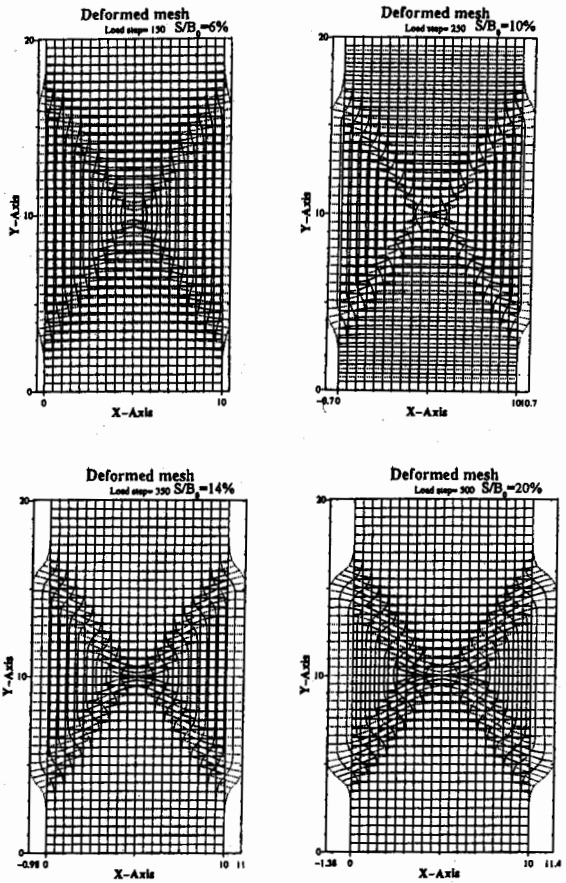

Fig 10. Sequential development of deformed mesh showing the formation of shear band for the case "f800".

CONCLUSIONS

The following conclusions can be drawn from the results and discussions presented above.

(1) Strain localization can be triggered in the simulation of a plane strain compression test due to the limitation of numerical precision.

(2) Reflective nature of strain localization occurs in case of symmetrically taken domain of analysis. As strain localization is very sensitive to the boundary, so reflection of localization happens at the line of symmetry.

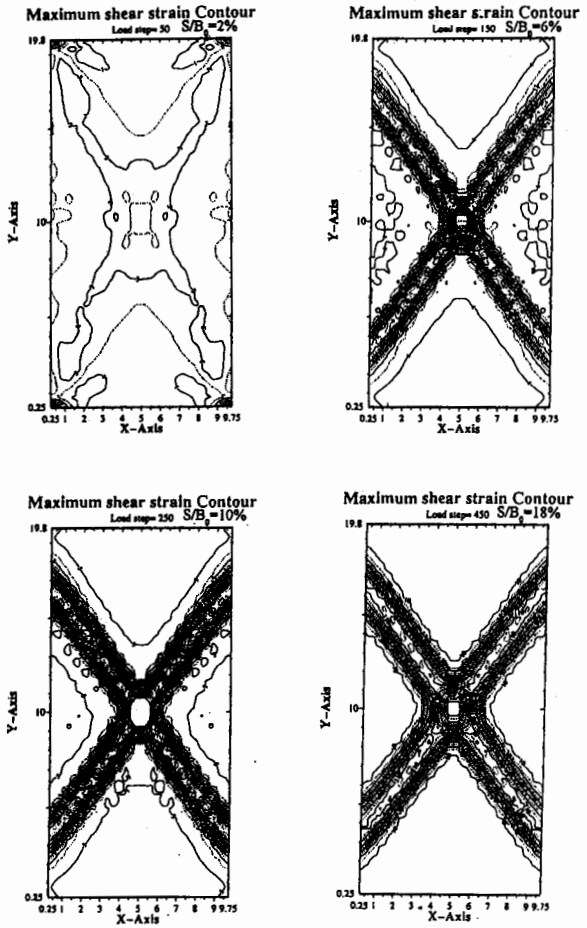

Fig 11. Sequential development of maximum shear strain, γ showing the formation of shear band for the case "f800".

(3) Strain localization or shear band depends on the smoothness or roughness of the loading boundary. Roughness or smoothness of top and bottom surface of a specimen in a PSC test simulation determines number of bands and orientation to some extent.

(4) This method of shear band analysis can be easily incorporated in any existing finite element code. This method does not involve any numerical difficulty unlike other sophisticated methods.

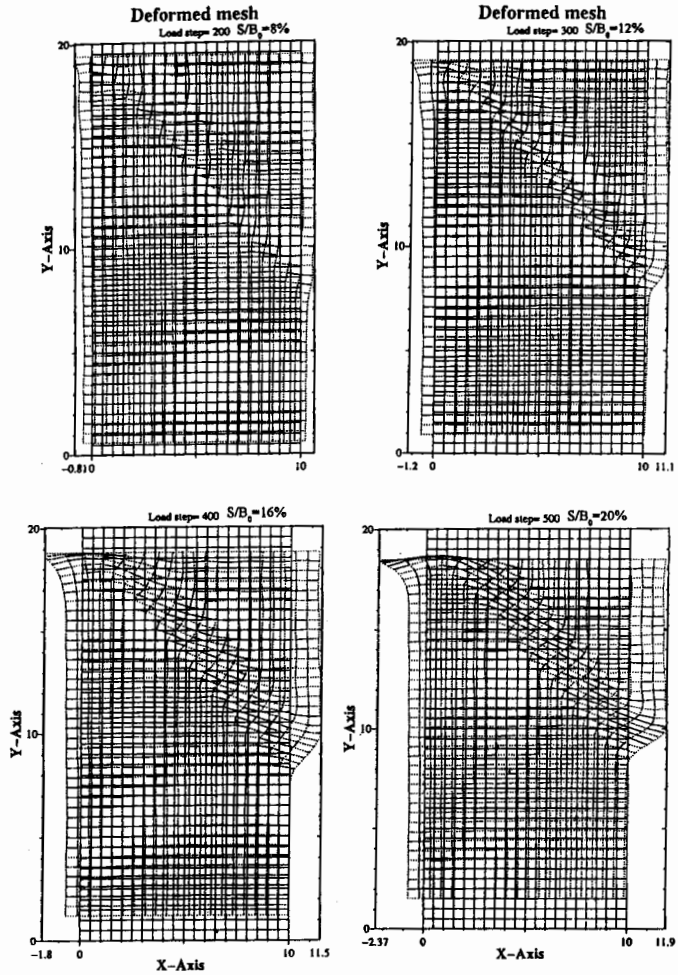

Fig 12. Sequential development of a single shear band in a deformed mesh for the case "f800s".

ACKNOWLEDGEMENT

The first author acknowledges gratefully the support provided by the Ministry of Education, Government, Science and Culture of Japan.

REFERENCES

Bazant, Z. P. and Oh, B. (1983), "Crack band theory for fracture of concrete", RILEM Mat. Struct.", No. 16, pp. 155-177.

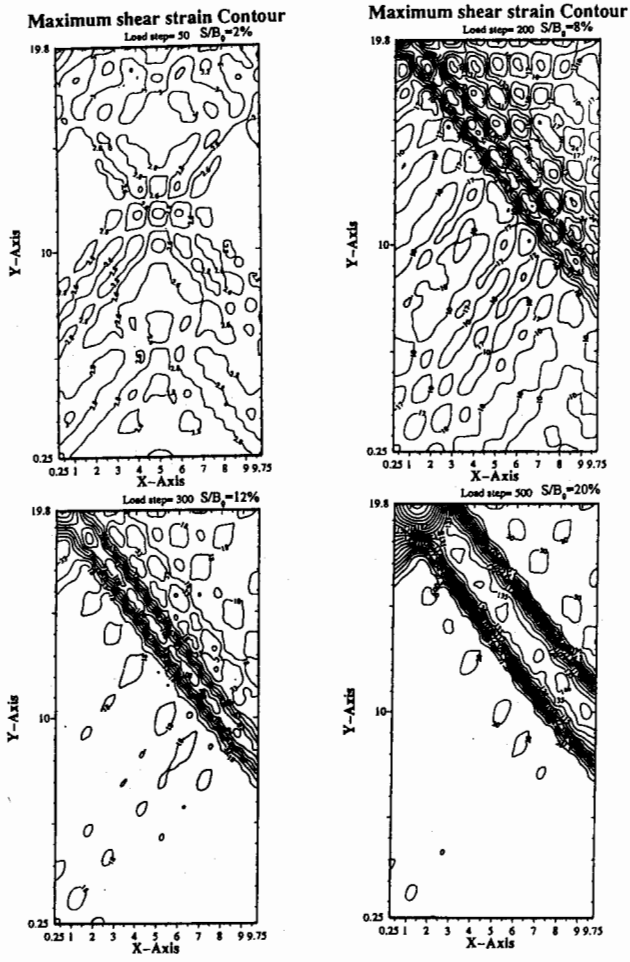

Fig 13. Sequential development of sshear strain, γ showing the formation of shear band for the case "f800s"

Bazant, Z. P., Belytschko, T. B. and Chang, T.-P. (1984), "Continuum theory for strain -softening", ASCE J. Eng. Mech., 110, pp. 1666-1692.

Bazant, Z. P. and Puaudier-Cabot, G. (1989), "Measurement of characteristic length of non-local continuum", ASCE J. Eng. Mech., 115, pp. 755-767.

Bazant, Z. P. and lin, F. (1988), "Nonlocal yield limit degradation", Int. J. Num. Meth. Eng., 26, pp. 1805-24.

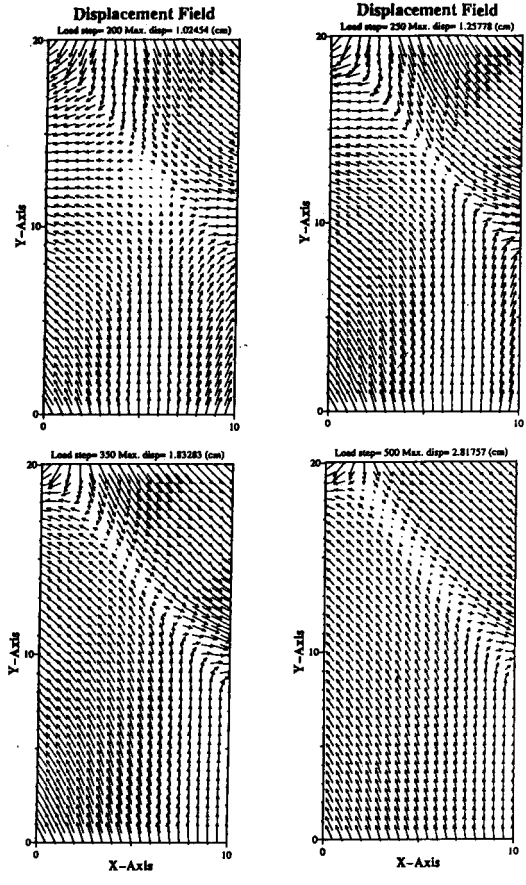

Fig 14. Sequential development of displacement vectors showing the formation of shear band for the case "f800s"

Bunce, J. W., (1972), " A Note on the Estimation of Critical Damping in Dynamic Relaxation", *Int. J. Numer. Methods Eng.*, 4, 301-304.

Cosserat, E. and Cosserat, F. (1909), "Theorie des Corps deformables" Herman et fils Paris.

Eringen, A. C. and Edelen, D. G. B., (1972), "On Nonlocal Elasticity", Int. J. Eng. Sci., No. 10, pp. 233-248.

Flanagan, D. P. and Belytschko, T., (1981), "A uniform strain hexahedron and quadrilateral with orthogonal hourglass control", *Int. J. Numer. Methods Eng.*, 17, 679-706.

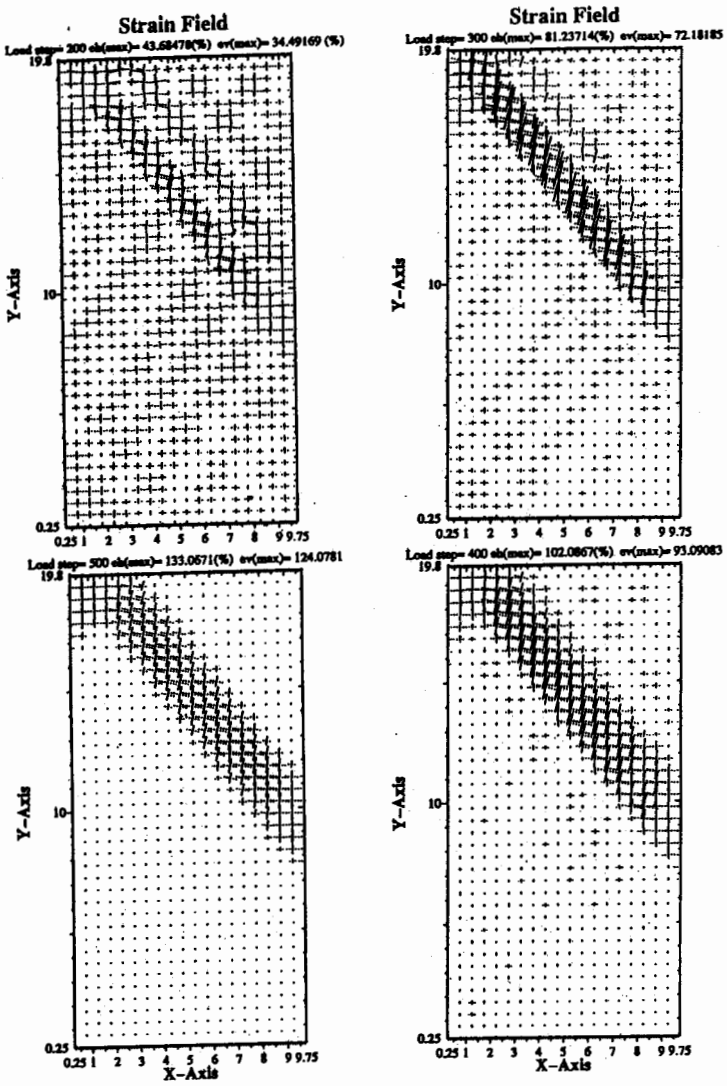

Fig 15. Sequential development of strain field (principal strains) showing the formation of shear band for the case "f800s"

Heinstein, M. W. and Yang, H. T. Y., (1992), "Plane strain finite element simulation of shear band formation during metal forming", *International Journal for Numerical Methods in Engineering*, Vol. 33, pp. 719-737.

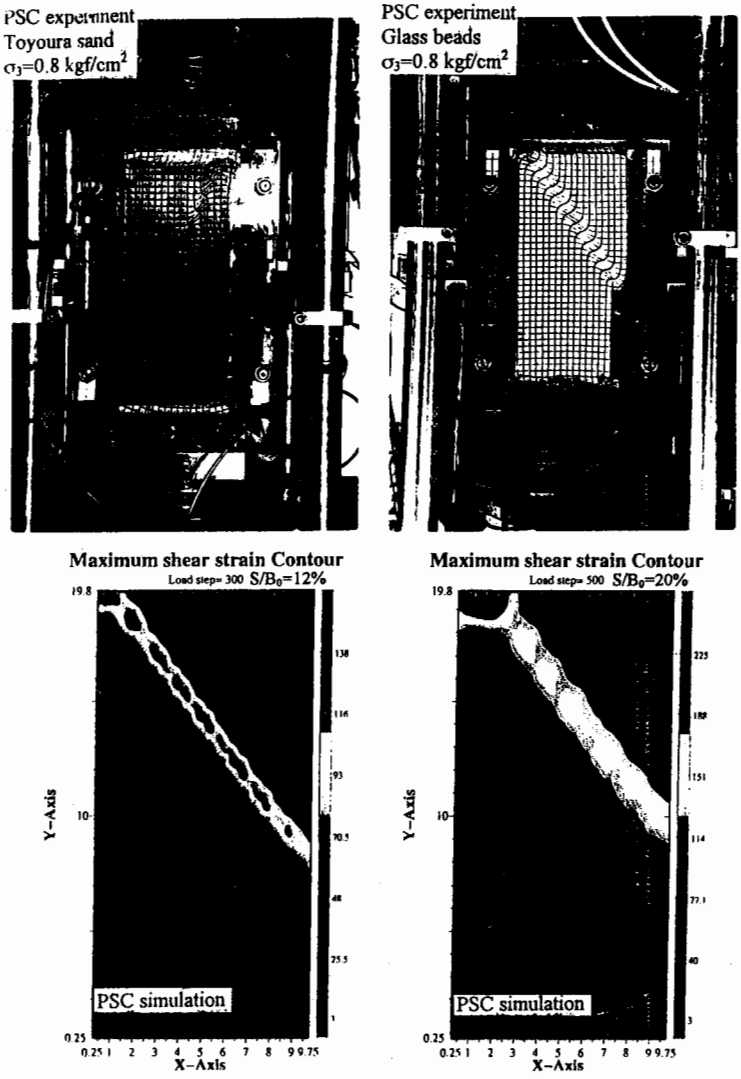

Fig 16. Comparison of FEM simulated shear band with that of PSC experiment. [color map ---> converted to B/W]

Gunther, W., (1958), "Zur Statik and Kinematik des Cosseratschen Kontinuums", Abh. Braunschweig. Wiss Ges., 10, pp. 195-213.

Key, S. W., Stone C. M. and Kreig, R. D., (1982), "Dynamic Relaxation Applied to the Quasi-static, Large Deformation, Inelastic Response of Axisymmetric Solids", in W. Wunderlich, E. Stein, K.-J. Bathe, *Nonlinear Finite Element Analysis in Structural Mechanics, Proceedings of the*

Europe U.S. Workshop, Ruhr-Universitat Bochum, Germany, July 28-31, pp. 585-620.

Loret, B. and Prevost, J. H. (1990), "Dynaic strain localization in elasto-(visco-) plastic solids, Part 1. General formulation and one-dimensional examples, Comp. Meth. Appl. Mech. Eng., 83, pp. 247-273.

Muhlhaus, H. - B. and Vardoulakis, I. (1987), "The thickness of shear bands in granular materials", Geotechnique, 37, pp. 271-283.

Muhlhaus, H.-B. and Aifantis, E.C. (1991), "A variational principle for gradient plasticity", Int. J. Solids Structures, 28, pp. 845-858.

Needleman, A., (1988), "Material rate dependence and mesh sensitivity on localization problems", *comp. Meth. Appl. Mech. Eng., Vol. 67, pp. 69-86.*

Ortiz, M. and Simo, J. C., (1986), *"An analysis of a new class of integration algorithms for elasto-plastic constitutive relations", Int. J. Numer Methods Eng.*, 23, pp. 353-366.

Pietruszczak, ST. and Mroz, Z., (1981), "Finite element analysis of deformation of strain softening materials", *Int. J. Numer. Methods Eng.*, 17, pp. 327-334.

Ramesh, G. and Krishanmoorthy, C. S., (1993), "Post-buckling analysis of structures by Dynamic Relaxation", *Int. J. Numer. Methods Engg.*, 36, pp. 1339-1364.

Rowe, P. W., (1962). "The Stress Dilatancy Relation for Static Equilibrium of an Assembly of Particles in Contact", *in Proceedings of Royal Society*, London, series A, pp. 500-527.

Siddiquee, M.S.A., (1991), "Finite element analysis of settlement and bearing capacity of footing on sand", Master' s' thesis, The University of Tokyo.

Tanaka, T. and Kawamoto, O., (1988), "Three dimensional finite element collapse analysis for foundations and slopes using dynamic relaxation", in Proceedings of *Numerical Methods in Geomechanics*, Insbruch, pp. 1213-1218.

Tatsuoka, F., Nakamura, S., Huang, C. C., and Tani, K., (1990), "Strength anisotropy and shear band direction in plane strain tests of sand", Soils and Foundations, Vol. 30, No. 1, pp. 35-56

Tatsuoka, F., Okahara, M., Tanaka, T., Tani, K., Moromoto, T. and Siddiquee, M. S. A., (1991), "Progressive failure and particle size effect in bearing capacity of a footing on sand", Geotechnical Engineering

Congress - ASCE, Geotechnical Special Publication 27, Vol. 2, pp. 788-802.

Tatsuoka, F., Siddiquee, M. S. A. Park, C.-S., Sakamoto, M. and Abe, F., (1993), "Modelling stress-strain relations of sand", Soils and Foundations, Vol. 33, No. 2, pp. 60-81.

Underwood, P. G., (1983), "Dynamic Relaxation A Review", in Belytschko T. and Huges T. J. R. (eds.), *Computational Methods for Transient Dynamic Analysis*, Chapter 5, North-Holland, Amsterdam.

Vermeer, P. A. and de Borst, R. (1984), "Non-associated plasticity for soils, concrete and rock", *Heron*, 29(3), 1-64).

Willam, K.J. (1984), "Experimental and computational aspects of concrete failure", Proc. Int. Conf. Computer Aided Analysis and Design of Concrete Structures, Eds. F. Damjanic et al,. Pineridge Press, Swansea, pp. 33-70.

Wu, F. H. and Freund, L. B., (1984), "Deformation trapping due to thermoplastic instability in one-dimensional wave propagation", J. Mech. Phys. Solids, 32(2), pp. 119-132.

Zienkiewicz, O. C., *The Finite Element Method*, McGraw-Hill New York, N.Y., 1984.

Zienkiewicz, O. C., Taylor, R. L. and Too, J M. (1971), "Reduced integration technique in general analysis of plates and shells", Int. J. Numer. Methods Eng., 3, 275-290.